

A Simple Model for Sheddies: Ocean Eddies Formed from Shed Vorticity

O. R. SOUTHWICK, E. R. JOHNSON, AND N. R. McDONALD

Department of Mathematics, University College London, London, United Kingdom

(Manuscript received 22 December 2015, in final form 26 May 2016)

ABSTRACT


Recent studies show that vertical eddy diffusivity is sufficient on its own to introduce intense horizontal shear layers at sloping ocean margins (Molemaker et al.; Gula et al.; Dewar et al.). These layers influence mesoscale energy and potential vorticity budgets but cannot be fully represented in models without sloping boundaries, no-slip boundary conditions, and sufficiently high resolution. This paper investigates the detachment of these shear layers and their subsequent rolling up into concentrated eddies. These shed eddies, or “sheddiess,” may have significant oceanographic impacts. Their growth is considered using a simple point vortex model that adapts the Brown–Michael model of vortex shedding to quasigeostrophic flow and allows detailed consideration of the vorticity fluxes. The model shows good qualitative agreement with observations and experimental and numerical results. It is applied to a number of examples of well-known cases of sheddy formation, including the Agulhas cyclones, California Undercurrent, and Canary Eddy Corridor, and also is used to investigate the effects of shed vorticity in the growth of the Cook Strait eddy and the interaction of the North Brazil Current rings with the islands of the Lesser Antilles.

1. Introduction

Since the large horizontal length scales of oceanic flows give Reynolds numbers typically of the order of 10^{11} , viscous effects are generally negligible. Exceptions occur in thin boundary layers, which can nevertheless be highly important. In typical ocean models, boundary layers at lateral boundaries are assumed insignificant and only the much thinner boundary layers on the upper and lower boundaries are considered. Recent work (Molemaker et al. 2015; Gula et al. 2015; Dewar et al. 2015) considers the effect of the turbulent bottom boundary layer over sloping bathymetry and demonstrates that the vertical shear in the bottom boundary layer necessarily implies a horizontal shear as well. Importantly, this effect does not require horizontal viscosity; the vertical eddy viscosity introduces horizontal shear. Full representation of these horizontal shear layers requires including sloping boundaries, no-slip

boundary conditions, and the required resolution, which is not achieved in most global models. Molemaker et al. (2015) estimate the horizontal scale of the boundary layer in the California Undercurrent as 200 m or less. Such fine features are not accurately resolved even in the finest of their three nested grids.

Provided the shear layers remain attached to the lateral boundaries, low horizontal diffusivity means that their vorticity remains confined to the boundary and does not influence the interior flow. However, if the shear layer detaches at a point of adverse pressure gradient or at a sharp change in direction of the boundary, vorticity is ejected from the layer into the interior of the fluid and can become dynamically significant in the interior flow. It is the aim of this paper to model the effect of the ejection of boundary vorticity. This tackles directly the difficulty of achieving realistically large Reynolds numbers in numerical ocean models. Vorticity diffusion is negligible in the bulk of the flow away from the boundaries, and so a simple model that tracks vorticity in the interior flow can accurately model many aspects of the flow. While the method here is not intended for direct implementation in ocean models, it aims to establish a foundation for

 Denotes Open Access content.

Corresponding author address: Oliver Southwick, Department of Mathematics, University College London, Gower St., London, WC1E 6BT, England.
E-mail: oliver.southwick.11@ucl.ac.uk



This article is licensed under a [Creative Commons Attribution 4.0 license](https://creativecommons.org/licenses/by/4.0/).

techniques explicitly representing sheddy formation in the ocean, demonstrating their value in a number of cases. It is hoped that the understanding built from these results can form the basis of future predictive investigations of sheddy formation.

Molemaker et al. (2015) run detailed nested grid simulations using the Regional Ocean Modeling System (ROMS). An example of one of their high-resolution simulations of the Californian Undercurrent is shown in Fig. 1. The shear layer can be seen attached to the wall in the bottom right of the figure with its strong negative vorticity colored dark blue. As the current flows northward past the headland at Point Sur the shear layer detaches, shedding vorticity into the main flow. The instabilities of this layer of vorticity initially form a number of small eddies before rolling up into a single large eddy. The present study builds on the work of Dewar, Molemaker, McWilliams, and Gula by modeling the evolution of the detached shear layer into a coherent shed eddy or “sheddy.”

Sheddies are commonly found near islands, for example, the Canaries, Seychelles, or Izu Islands (Sangrà et al. 2007; Heywood et al. 1996; Isoguchi et al. 2009), all of which lie in the path of strong currents. The Canaries, for example, form a barrier disrupting the southwestward flow of the Canary Current and shed eddies continuously. These eddies initially move southwestward with the current before turning west under the influence of the β effect. The chain of mesoscale eddies this produces, known as the Canary Eddy Corridor, has been estimated to be responsible for around a quarter of the mass transport and half of the kinetic energy transport of the Canary Current (Sangrà et al. 2009).

Another common origin for sheddies is sharply varying coastlines such as capes (Jiang et al. 2011). An example of this are the sheddies formed on the leeward side of the Agulhas bank (Penven et al. 2001). These sheddies play an important role in triggering the formation of the Agulhas rings (Lutjeharms et al. 2003)—the main interchange mechanism between the Indian and Atlantic Oceans. Sheddies can also be formed from both eastern (Molemaker et al. 2015) and western (Gula et al. 2015) boundary currents. Here, highly asymmetric distributions of cyclonic and anticyclonic eddies are observed when the boundary layer separates at points along the coast with particularly high curvature.

The separation of shear layers may have impacts on other ocean processes as well. A potentially important example is the impact of sheddies on other eddies encountering topography such as the North Brazil Current (NBC) rings meeting the islands of the Lesser Antilles (Fratantoni and Richardson 2006). Numerical (Simmons and Nof 2002) and experimental

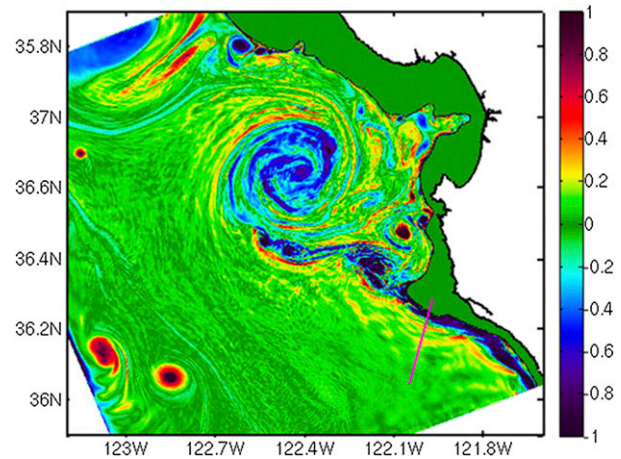


FIG. 1. Normalized relative vorticity in the California Undercurrent showing the shear layer separating at Point Sur from the ROMS simulation of Molemaker et al. (2015). The magenta line simply indicates the position of a transect discussed by Molemaker et al. (2015), but is not of relevance here.

(Duran-Matute and Velasco Fuentes 2008; Tanabe and Cenedese 2008) investigations have seen flow separation around the Lesser Antilles as a NBC ring approaches. Additionally many smaller eddies that may have separation of shear layers as their origin have been observed in the paths of buoys to the west of the islands (Richardson 2005). The present model enables us to investigate the role of sheddies in determining the trajectories and survival rate of the NBC rings. There are also cases of eddies, such as the Cook Strait eddy, whose origin is unknown (Barnes 1985). It is suggested here that vorticity ejected from a boundary shear layer could be the source of these eddies.

Although oceanic flows have very high Reynolds number, the highly coherent eddies observed in the lee of islands match well to numerical experiments that show that, for rotating, stratified flows, coherent vortices are found for all values of the Reynolds number (Dong et al. 2007). However, it may not be possible to apply standard results from the wake of a cylinder to all island shapes. Observations of island wakes with differing flow direction, but otherwise similar conditions, show significantly different wakes (Heywood et al. 1996), suggesting that it is important to consider the coastal shape. This work therefore considers a number of examples of different coastal shapes representing different oceanic scenarios. Klinger (1994) examined the formation of eddies on the leeside of a cape in two-layer rotating tank experiments, finding that sheddies formed for cape angles less than 135° .

Simple, low-order models have many important strengths when considering the dynamics of ocean eddies. Many eddies are below the grid size of large-scale ocean

models but are still dynamically important, meaning that their effects must be parameterized. Modeling helps build effective and physically appropriate parameterizations. It is often not possible to achieve realistically large Reynolds numbers in numerical ocean models, and indeed it may not be necessary. An appropriate alternative approach to modeling extremely high Reynolds number flow may be to use inviscid models with no interior viscous effects and boundary viscous effects represented solely by their vortical dynamics. Low-order models are generally quicker and cheaper to implement than more sophisticated alternatives and have the advantages of being easier to understand and of isolating and highlighting the key physical processes involved.

Simple models may even have a role to play in global, numerical models. Representations of emerging tropical cyclones in weather models have been significantly improved by explicitly adding “bogus” or “synthetic” vortices to model the initial formation of cyclonic features (Kurihara et al. 1993, 1995; Chou and Wu 2008; Hsiao et al. 2010). This method reduces errors introduced by limited horizontal resolution and enables the placement of vortices at observed storm positions. When considering oceanic flow separation, the question naturally arises as to where such features would be placed or how strong they would be, and the model here addresses these questions.

A simple approach to modeling flow separation is to focus on the developing core of vorticity as the most dynamically important feature and represent this as a single-point vortex. The strength of this vortex increases as the vorticity leaves the boundary layer at the separation point and rolls up. The vorticity distribution is determined by requiring that the velocity remain finite at the separation point: a Kutta condition. Irrotational flow of inviscid fluid around a corner has infinite velocity at the corner. The presence of even infinitesimal viscous effects at sufficiently high Reynolds number means the flow separates at the corner. In the model here, the vorticity shed at the corner is taken to roll up into a point vortex whose strength increases continuously, following Brown and Michael (1954), who derived an equation of motion for the location of a shed eddy through a force balance argument.

The Brown–Michael model has been shown to capture the qualitative features of high Reynolds number, two-dimensional, incompressible, nonrotating flows and has been used, and further developed, extensively (Rott 1956; Graham 1983; Cortezzi and Leonard 1993). As well as traditional applications in aeronautics (Manela and Huang 2013), it has been applied to a variety of problems such as coupled solid–fluid interactions (Michelin

and Llewellyn Smith 2010), swimming (Ysasi et al. 2011), and biological models such as ventricle filling (Pedrizzetti 2010). The model shows good qualitative agreement with both experimental results (Blondeaux and De Bernardinis 1983), more sophisticated models (Sheng et al. 2011), and high-resolution numerical simulations (Eldredge and Wang 2010) in a variety of flow situations. Southwick et al. (2015) adapted the Brown–Michael model for oceanic flows by introducing quasigeostrophic dynamics and the effects of the deforming free surface instead of classic two-dimensional potential flow. It is this quasigeostrophic Brown–Michael (QGBM) equation that will be used here to model the formation of sheddies in a number of oceanographic contexts.

Section 2 introduces the model and techniques. Section 3 discusses a boundary current along a stepped coastline in relation to the California Undercurrent passing Point Sur modeled here as a backward-facing step. The model allows a straightforward discussion of the rate of expulsion of vorticity into the fluid and its subsequent rolling up into an eddy. Section 4 models the sheddies formed in the lee of the Agulhas bank as flow around a wedge. Section 5 examines eddies formed at gaps in barriers and is split into three subsections, each considering a different oceanographic scenario. Section 5a models the flow through Cook Strait and investigates whether flow separation could explain the large, trapped eddy found at the mouth of the gap. Section 5b investigates the interaction of North Brazil Current rings with the islands of the Lesser Antilles. Section 5c discusses the Canary Eddy Corridor, a chain of sheddies formed at the Canary Islands but extending far out into the Atlantic. Section 6 presents conclusions.

2. The quasigeostrophic Brown–Michael model

The flows considered here are shallow with horizontal length scales of tens of kilometers and time scales of days or weeks. For simplicity, the flow is thus modeled as a 1.5-layer quasigeostrophic flow with the active layer containing any vortices and passive layers above or below, depending on the scenario under consideration. The analysis follows closely that of Southwick et al. (2015) and so will only be discussed briefly.

The interface perturbation η is a streamfunction for the flow, and so the fluid velocity $\mathbf{u} = (u, v)$ is given by

$$\mathbf{u} = \left(-\frac{\partial\eta}{\partial y}, \frac{\partial\eta}{\partial x} \right), \quad (1)$$

where $\mathbf{x} = (x, y)$ are the horizontal spatial coordinates. The potential vorticity (PV) is taken to be zero

throughout the flow except at the locations $\mathbf{x}_i(t)$ of a finite number of point vortices with strengths $\Gamma_i(t)$, giving the nondimensional equation for the surface perturbation (Hogg and Stommel 1985; Davey et al. 1993):

$$\nabla^2 \eta - \frac{1}{a^2} \eta = \sum_{i=1}^m \Gamma_i(t) \delta[\mathbf{x} - \mathbf{x}_i(t)], \quad (2)$$

where t is the time, a is the ratio of the Rossby radius of deformation to the length scale of the flow, m is the number of point vortices, and δ is a two-dimensional delta function. This two-dimensional, partial differential equation is known as the modified Helmholtz equation.

The model is closed by inverting (2) to obtain η and hence the velocity field \mathbf{u} from (1). The precise solution depends on the geometry of the flow field and the background flow determined by the boundary conditions. Subsequent sections discuss various forms of these boundary conditions and geometries in different oceanographic scenarios.

The propagation velocity of the i th vortex can be found from the nonsingular part $\tilde{\eta}_i$ of the streamfunction

$$\tilde{\eta}_i = \eta + \frac{\Gamma_i}{2\pi} K_0 \left(\frac{|\mathbf{x} - \mathbf{x}_i|}{a} \right), \quad (3)$$

where K_n is the modified Bessel function of the second kind of order n , the open-domain Green's function for the modified Helmholtz operator. The tilde and subscript i notation denotes that this is the streamfunction felt by the i th vortex. The velocity of a constant circulation vortex is then given by

$$\dot{\mathbf{x}}_i = \tilde{\mathbf{u}}_i = \lim_{\mathbf{x} \rightarrow \mathbf{x}_i} \left(-\frac{\partial \tilde{\eta}_i}{\partial y}, \frac{\partial \tilde{\eta}_i}{\partial x} \right). \quad (4)$$

However, in the Brown–Michael model, the circulation of the shed vortices changes to satisfy the Kutta condition at the separation point. That is, the circulations adjust so as to keep the velocity finite at any sharp corners on the boundary of the domain. The increasing vortex circulation exerts an additional force on the point vortex and the infinitesimal sheet of vorticity connecting the vortex to the separation point. To balance this force, an additional term appears in (4), which in quasigeostrophic flow gives the QGBM equation (Southwick et al. 2015):

$$\dot{\mathbf{x}}_i = \tilde{\mathbf{u}}_i - \frac{\dot{\Gamma}_i}{\Gamma_i} \frac{\mathbf{x}_i}{|\mathbf{x}_i|} a \int_0^{|\mathbf{x}_i|/a} s K_1(s) ds, \quad (5)$$

where $\dot{\Gamma}_i$ is the rate of change of circulation over time. This equation is derived by Southwick et al. (2015) from a force balance on the point vortex and connecting

vortex sheet, with the additional correction term due to the force integrated along the vortex sheet, and the integration variable s being the pathlength along the sheet. Note that (5) reduces to the usual vortex motion equation [(4)] when $\dot{\Gamma}_i = 0$ and the shed vortex has constant strength.

A commonly used and physically realistic additional condition, first applied by Graham (1980), is that the circulation of any shed vortex may only increase (and not decrease) in time as it is “fed” by the continuous shedding of vorticity from the separation point. If $\dot{\Gamma}_i$ changes sign, the vortex is cut off, its circulation is frozen, and it continues as a free vortex with a new shed vortex created at the separation point. This new vortex necessarily has opposite-signed circulation to the cutoff vortex. In practice, it is computationally simpler to limit the number of new vortices when adding vortices would do little to change the overall dynamics. Therefore, a practical amendment to the Graham (1980) condition is to introduce a new vortex only when the decrease in circulation is significant, avoiding introducing a large number of new vortices when the shed vorticity fluctuates rapidly with small amplitude. The computations here introduce a new vortex if the shed circulation decreases by 5% from its maximum value.

For very large shed eddies, far from the separation point, instabilities in the vortex sheet connecting the sheddy to the separation point start to dominate, destroying the vortex sheet and stopping the growth process. This can be represented in the QGBM model by cutting off a shed vortex and starting a new vortex if the shed vortex meets some condition. Appropriate choices could be some maximum circulation or a maximum distance from the separation point. This is particularly relevant for vortices shed from the edges of a gap, which form pairs and then propagate as a single entity. At this point they are no longer being fed by the separation point vorticity. These pairs are thus modeled here as free vortices when the distance between the two vortices forming the pair is shorter than the distance from the vortices to their separation points. Section 5c discusses these criteria and their effects.

The biggest challenge in implementing these equations is computing the streamfunction efficiently. Southwick et al. (2015) describe a scheme based on conformally mapping the flow domain to the upper half plane to eliminate velocity singularities and solving with a Chebyshev spectral method. If a map from the physical domain (coordinates $z = x + iy$) to a simpler computational domain (coordinates $Z = X + iY$) is known, then the problem can be solved in this

computational domain. The open-domain solution of the inhomogeneous part of (2) (the direct contribution from the point vortices) is

$$\eta = - \sum_{i=1}^m \frac{\Gamma_i}{2\pi} K_0 \left(\frac{|\mathbf{x} - \mathbf{x}_i|}{a} \right). \quad (6)$$

Under the mapping, the homogeneous part of (2) (which enforces the boundary conditions) becomes

$$\nabla_Z^2 \eta - \frac{1}{a^2} \left| \frac{\partial z}{\partial Z} \right|^2 \eta = 0, \quad (7)$$

where ∇_Z^2 denotes the Laplacian $\partial^2/\partial X^2 + \partial^2/\partial Y^2$. This can be solved in the computational domain, and derivatives (and therefore velocities) can be found in the physical domain using the Jacobian $\partial(X, Y)/\partial(x, y)$. The ordinary differential equations for the vortex positions are integrated either using standard Runge–Kutta schemes or the implicit time-stepping scheme described by Southwick et al. (2015).

3. Flow over a backward-facing step—eddy formation in the California Undercurrent

Boundary currents such as the California Undercurrent are a ubiquitous feature in the oceans. The California Undercurrent is a northward-flowing subsurface current extending 100 km from the coast, reaching speeds of more than 0.1 m s^{-1} between depths of 100 and 400 m (Collins et al. 2000) and is part of a typical subtropical eastern boundary current. It develops a narrow strip of negative vorticity due to the turbulent bottom boundary layer and bottom stress. At several points along the coast, this shear layer separates and the vorticity is ejected into the main flow, forming eddies. This can be seen in the numerical results of Molemaker et al. (2015) reproduced in Fig. 2. Here, the headland of Point Sur is the catalyst for the separation of the shear layer detaching from the coast. The shear is unstable and rolls up into a number of smaller eddies before being wound into a single large core of vorticity. These strong anticyclonic eddies, known as “cuddies,” have been frequently observed in the region (Dewar et al. 2015). Downstream of Point Sur, there is a return flow along the coast that generates positive vorticity, seen in red in Fig. 2. This shear layer is not as large or strong, as it has had less time to develop, and the return flow is weaker than the upstream current. A small eddy of positive circulation can be seen just past Point Sur in Fig. 2. This could have been formed in a secondary separation of this positive vorticity layer, a common feature observed in separated flows. The California

Undercurrent serves as an illustrative example of the formation of sheddies in a boundary current. In general, the number of eddies formed may depend sensitively on details of the shape of the coastline that may be below the grid scale in some large-scale models. Simple models thus have an important role in describing these local processes for global models.

To apply the QGBM model to the California Undercurrent at Point Sur, the coastline [with coordinates (x_c, y_c)] is represented as a backward-facing step formed by three sections of coast: $x_c < 0, y_c = 1$; $x_c = 0, 0 < y_c < 1$; and $x_c > 0, y_c = 0$, with flow in $y > y_c$, as can be seen in Fig. 3 (where the view is rotated about the origin for ease of comparison with Fig. 2). A suitable choice of mapping between this physical domain and a computational domain is

$$z = \frac{\sinh Z - Z}{\pi}, \quad (8)$$

which takes the three lines that make up the physical coast to the three sides of the semi-infinite strip $0 < X, -\pi < Y < 0$, which can then be truncated for computational purposes to a rectangle by choosing $0 < X < L_r$, for some truncation length L_r . The truncation distance in the physical domain increases exponentially with L_r . Care must be taken near the corner at $(0, 1)$, which is mapped from an angle of $3\pi/2$ to $\pi/2$. Near the image of this point in the mapped domain,

$$\eta \sim c_0 + c_2 Z^2 + O(Z^3) \quad (9)$$

for constants c_0 and c_2 . The constant c_2 is required to satisfy the Kutta condition but, unlike in Southwick et al. (2015), cannot be found from the derivative of η at the origin; instead, the values of η near the origin must be used to find c_2 , using the form (9). Since η is a streamfunction for the flow, a steady flow of flux Q can be set up by requiring that $\eta \rightarrow 0$ far from the boundary and that $\eta = Q$ on the boundary.

The results of a simulation in which (5) and (7) are solved to find the evolution of an eddy shed by a steady flow ($Q = 1, a = 1$) as it passes the corner of a backward-facing step are given in Fig. 3, which shows the surface perturbation and shed vortex trajectory at four times. The center of the eddy can be seen as the largest surface elevation, the height of which grows over time, showing the increasing strength of the eddy. To show the path of the shed vorticity, passive tracers are continuously released, and their positions are shown in the first two panels. These are streaklines for the flow and show the shed vorticity winding up around the vortex. The shed vortex initially grows and drifts downstream in a similar way to the sheddy in Fig. 2. Over longer time,

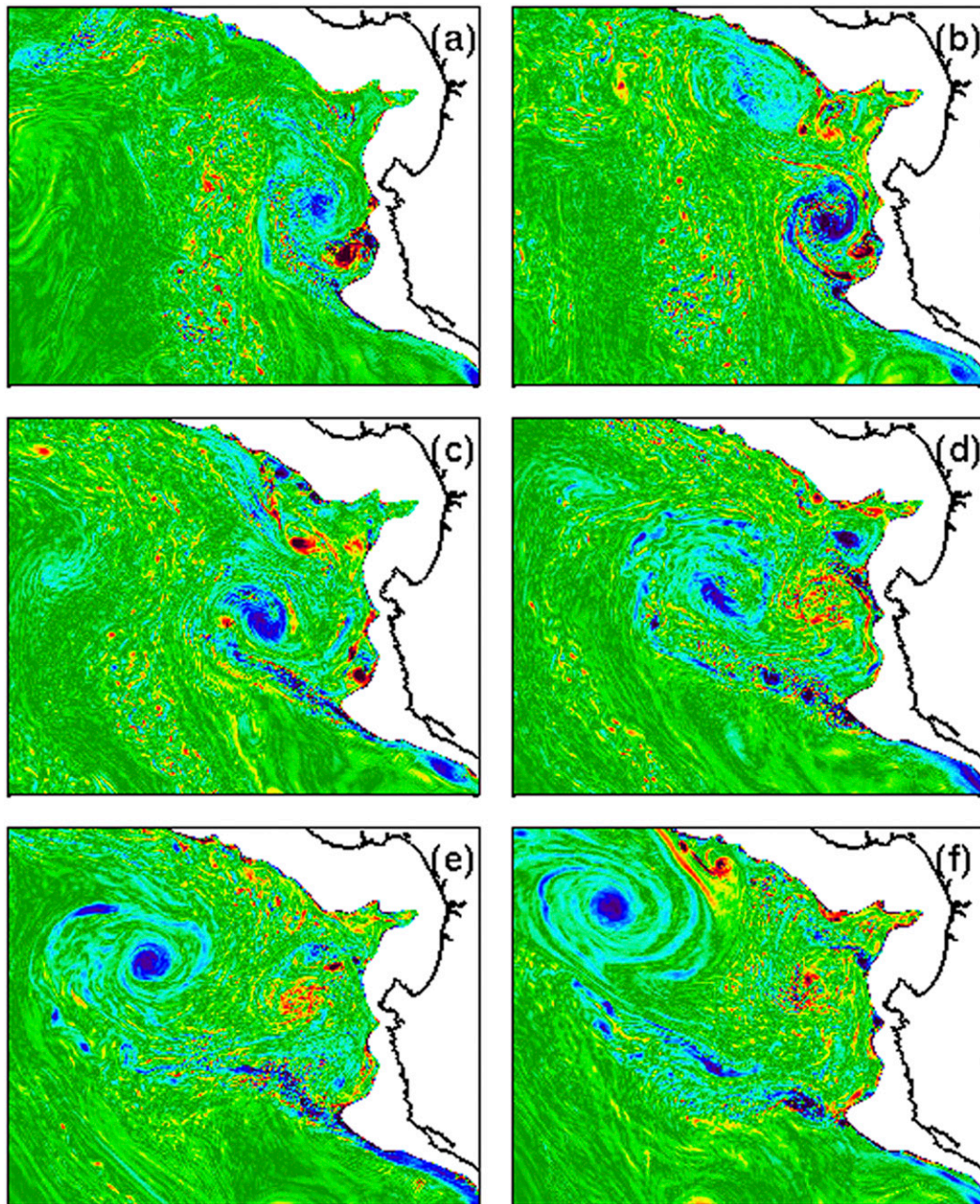


FIG. 2. Normalized relative vorticity showing the evolution of the detached shear layer, its instabilities, and roll up into a sheddy in a horizontal plane at 150-m depth from the ROMS simulations of the California Undercurrent past Point Sur reproduced from [Molemaker et al. \(2015\)](#).

the shed eddy slows and settles to a stationary state with a fixed location and constant circulation. Comparison of [Figs. 2](#) and [3](#) suggests that the QGBM model is qualitatively capturing the growth of the shed eddy.

The model allows discussion of the shedding of vorticity and its passage into the shed vortex in terms of the various vorticity fluxes. Vorticity is held in the boundary

layer, separates at the headland, and rolls up into a core. The vorticity in the separated sheet has two contributing components: negative vorticity held in the boundary layer at the edge of the oncoming flow and the positive vorticity held in the edge of the recirculating current on the lee side of the separation point. The negative upstream vorticity and positive recirculation vorticity are shed at the separation point and begin to cancel through

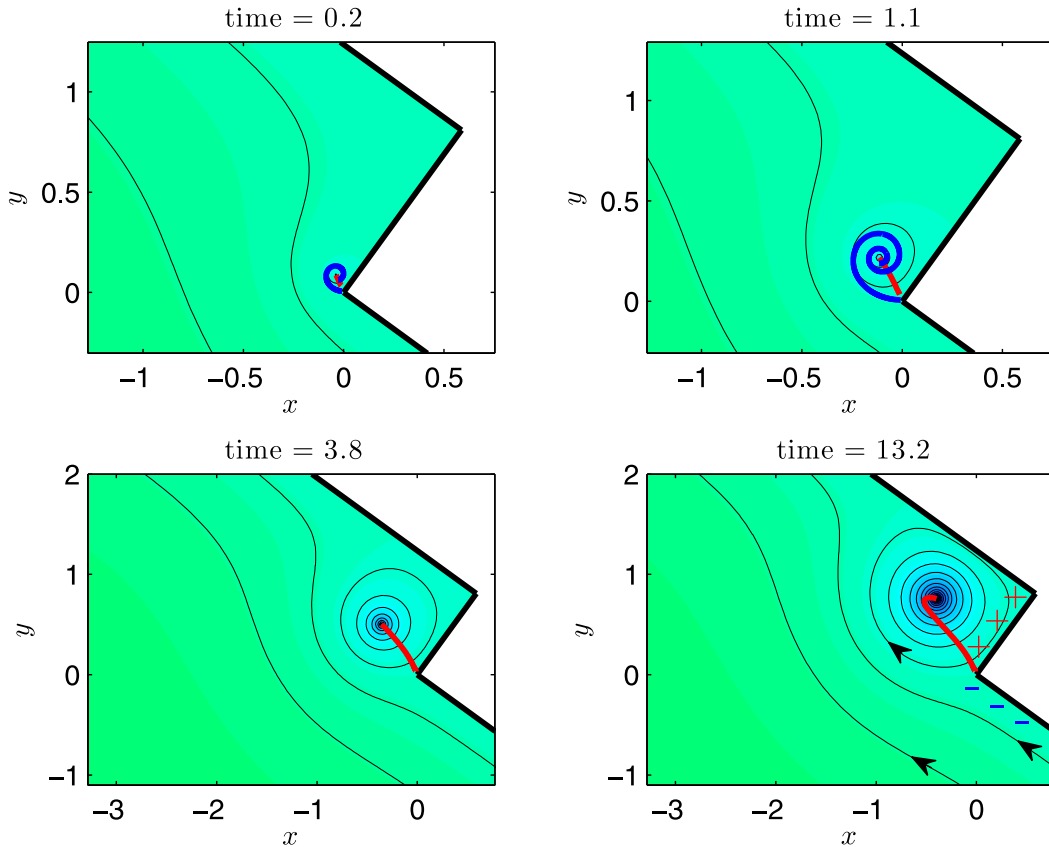


FIG. 3. The surface perturbation from a QGBM simulation showing the evolution of a sheddy forming in the lee of a backward-facing step. In this and all subsequent figures, blue and red show surface elevation and depression, respectively. The black lines mark contours of the surface perturbation at equal intervals, which are streamlines for the flow, and the vortex trajectory is shown in red. The first two panels show a closer view with streaklines in blue, showing the shed vorticity winding up into the vortex. In the final panel, the eddy has evolved to a steady state with fixed location and constant circulation. The signs indicate the sign of the vorticity in the upstream and recirculation boundary layers.

cross diffusion. This can be seen in the results of Molemaker et al. (2015), displayed in Fig. 2. The separated vortex sheet near the cape consists of both blue negative vorticity from upstream of the cape and red positive vorticity from downstream; however, farther along the sheet the two have mixed and cross diffused, leaving only the net negative vorticity to roll up into the eddy. Dewar et al. (2015) discuss the details of this process and the associated instabilities in the shed flow, which also lead to the enhanced mixing of vorticity.

These processes can be quantified in the QGBM model. Suppose that the boundary layer has thickness $O(\delta)$ and an inner velocity profile $\mathbf{u}'_l(x', y')$ matching an outer solution with speed $\mathbf{u}'(x', 0) = (U, 0)$ to zero velocity on the wall, where $\mathbf{x}' = (x', y')$ and $\mathbf{u}' = (u', v')$ are local coordinates and velocities tangential and normal to the wall, respectively. As the layer is thin, the leading-order vorticity in the layer is

$$\omega_l = \frac{\partial u_l}{\partial y} - \frac{\partial v_l}{\partial x} \approx \frac{\partial u_l}{\partial y}. \tag{10}$$

Therefore, the flux of vorticity along the boundary layer is

$$\int_0^\delta \omega u_l dy' \approx \int_0^\delta \frac{\partial u_l}{\partial y} u_l dy', \quad \text{and} \tag{11}$$

$$= \int_0^U u_l du'_l = \frac{U^2}{2}, \tag{12}$$

and depends only on the speed of the outer solution at the boundary. Thus, the vorticity fluxes at the separation point can be obtained and related to the growth of the shed eddy. The rate of change of sheddy circulation and the upstream recirculation and net vorticity fluxes are shown in Fig. 4. The boundary layer vorticity fluxes are evaluated away from the separation point as the velocity

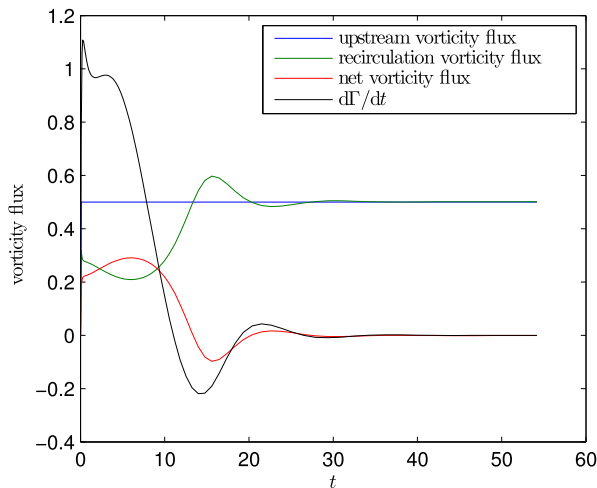


FIG. 4. The evolution of vorticity fluxes at the separation point and shed vortex for a QGBM simulation of a sheddy forming in the lee of a backward-facing step.

vanishes there. For the recirculation vorticity flux, the average of the vorticity fluxes from the reattachment point [the point where $v(0, y) = 0$] to the separation point is used, and for the upstream vorticity flux the far upstream values are used. Equation (12) models a shear layer that is quasi steady, which in the early stages of the evolution here may not be the case. Initially the recirculation flux may carry negative vorticity formed at earlier times back to the separation point.

Figure 4 shows that once the sheddy has evolved to its steady state, the vorticity fluxes balance perfectly; the fluxes of negative vorticity from upstream and positive recirculation vorticity are equal and opposite so the shed vortex grows no further. Earlier on in the evolution of the vortex, the increase in vortex circulation and the net vorticity flux follow the same pattern qualitatively but do not match exactly. As noted above, for early times the quasi-steady layer formulation of (12) may not be appropriate. Taking the vorticity in the recirculation shear layer at early times to be the upstream value of $-1/\delta$ gives an initial net vorticity flux of approximately 0.9, close to the rate of change of sheddy circulation of approximately 1. Using the velocity scale of 0.1 m s^{-1} (Molemaker et al. 2015), Rossby radius of 30 km (Chelton et al. 1998), and taking the typical length scale to be comparable to the Rossby radius gives a typical time scale of approximately 3.5 days. Thus, it appears that the majority of the eddy growth in Fig. 4 is complete within the first 30 days, with the vorticity fluxes settling to a balance from this point onward. The evolution in Fig. 2 spans a period of 35 days, a similar vorticity production time scale to that given by the QGBM model.

It appears that the QGBM model qualitatively represents the separated flow over a stepped coastline. Comparing the results here to simulations of the California Undercurrent (Molemaker et al. 2015) shows reasonable agreement in the shedding of the shear layer and its roll up into a concentrated core. At later times when the fluxes of vorticity come into balance, the sheddy settles to a steady position and ceases to grow in strength. If this result is robust, this steady state suggests that it may be possible to have an area of high vorticity trapped on the leeward side of a stepped coastline.

4. Flow around a cape: Agulhas cyclones

The Agulhas current is an intense western boundary current carrying a flux of 70 Sv ($1 \text{ Sv} \equiv 10^6 \text{ m}^3 \text{ s}^{-1}$) southwest along the east coast of Africa. As the Agulhas enters the South Atlantic, interaction with the Antarctic Circumpolar Current forces it to bend and flow eastward: the Agulhas retroflection. This retroflection is unstable and periodically produces large, anticyclonic eddies known as the Agulhas rings. Transport by these eddies is the main mechanism of interocean exchange between the Indian and South Atlantic Oceans, with estimates of their flux typically of the order of 10 Sv. They are a significant source of salt and heat in the South Atlantic Gyre.

Although the large-scale behavior is well documented, many details contribute to the interocean exchange between the Indian and Atlantic Oceans (Boebel et al. 2003). For example, cyclonic eddies formed by separation in the lee of the Agulhas Bank are found in both observational (Lutjeharms et al. 2003) and numerical (Penven et al. 2001) studies. Figure 5 shows one of these eddies observed in satellite sea surface height data from Lutjeharms et al. (2003), who note that these eddies are often important in the formation of the larger, anticyclonic Agulhas rings.

The initial growth of an Agulhas cyclone is modeled here as a representative example of an eddy formed from a detached flow at a cape. The Agulhas Bank is represented as a right-angled wedge (the solution for arbitrary angle follows similarly). The current is taken to be a simple, steady, westward flow around the cape tip of flux Q , imposed with the boundary conditions $\eta = Q$ on the coast and $\eta \rightarrow 0$ far from it. The results of this simulation with $Q = 1$ are shown in Fig. 6. Here, the Rossby radius L_r can be used as the length scale L , so all solutions are a rescaling of the $a = 1$ solution. The surface height is displayed at three times, and the trajectories of two passive markers are included. The marker trajectories over each time period are shown as white lines with a white circle, indicating their final position.

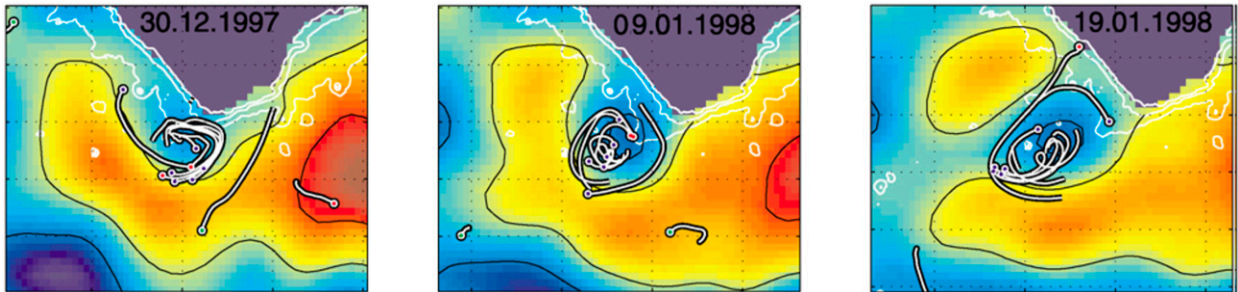


FIG. 5. An Agulhas cyclone shown in sea surface height data from Modular Ocean Data Assimilation System (MODAS)-2D. Trajectories of several RAFOS floats are shown in white with circles denoting their final positions. Reproduced from Lutjeharms et al. (2003).

The eddy drifts away from the coast as it grows on the leeward side of the bank. Both the evolving location and increasing strength of this eddy bear reasonable qualitative resemblance to the observations shown in Fig. 5. The paths of the passive tracers in Figs. 5 and 6 also appear qualitatively similar, suggesting that passively advected particles around a growing shed vortex may be a good representation for the dynamics of these buoys, even though the point vortex simulations cannot capture the full variability present in Fig. 5.

Penven et al. (2001) compare high-resolution numerical simulations to observations of sheddies forming in the lee of the Agulhas Bank. They take averaged values of the Rossby ($Ro = 0.04$) and Burger ($S = 3.8$) numbers computed by Boyer and Tao (1987), use the width of the Agulhas Current (100 km) as a characteristic length scale, and have currents of order 1 m s^{-1} . As the Rossby number is small, the QGBM model is appropriate. Using these parameter values gives a number of dimensional predictions that can be compared to observations.

In the QGBM results, the eddy grows rapidly in strength over a period of approximately 30 days, with this growth then plateauing (growing only a further 10% over the next 30 days). The eddy is expected to detach once its circulation has ceased growing

significantly and so may detach somewhere in the range of 30–90 days after its initial formation, giving an estimate of 4–12 eddies shed per year, consistent with the results of Penven et al. (2001) showing 3–5 eddies forming per year and the observations of Lutjeharms et al. (2003) showing a sheddy growing over a period of approximately a month. The movement of the eddy also slows after the initial growth, and it settles at a distance of approximately 200 km from the cape, comparable with the distance of 300 km found in Penven et al. (2001). Current speeds between a third and a whole Rossby radius from the eddy center lie in the range $0.5\text{--}2.5 \text{ m s}^{-1}$, larger than, but again comparable with, the float velocities of around 0.5 m s^{-1} found by Lutjeharms et al. (2003). The QGBM model thus predicts values of the same order as those in observations and high-resolution simulations.

Although the surface perturbation is singular at the center of the vortex, the singularity is integrable so the entire vortex has finite volume, and quantities such as volume and average surface perturbation can be predicted. Using the Rossby radius as the length scale and a typical reduced gravity value of 10^{-2} m s^{-2} , the average surface perturbation within the core of the vortex (within one Rossby radius from the center) can be calculated by integrating the known surface perturbation to

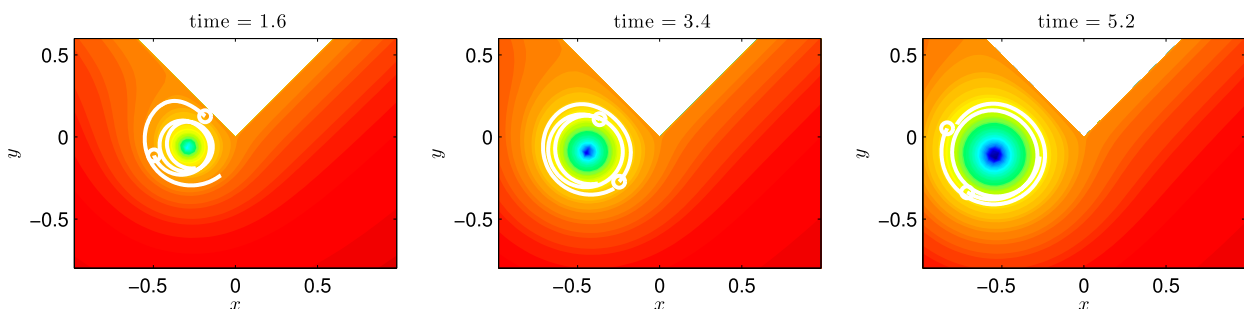


FIG. 6. The surface perturbation for a QGBM vortex growing from the tip of a right-angled wedge at three times for $Q = 1$ and $a = 1$. Trajectories of two passive marker floats are shown in white with circles denoting their final positions.

give the volume and then dividing by the horizontal area. This gives an estimated average surface perturbation of 100 m for Agulhas cyclones, the same order of magnitude as the perturbations shown in Fig. 3 of Penven et al. (2001).

5. Flow through a gap

a. Unidirectional flow through a gap: The Cook Strait

The two largest islands of New Zealand form a 1400-km north–south barrier to the prevailing winds and currents. The only gap in this barrier is Greater Cook Strait, just 24 km across at its narrowest point. As Walters et al. (2010) note, the flow in the Greater Cook Strait region is complex with many influencing factors: the meeting of several currents, complex and dramatic topography and bathymetry, wind forcing, tidal stresses, density variations, sea level differences, and river discharges. Different factors dominate in different areas of the strait, and so building a full understanding of the currents in the region requires piecing together many factors.

Walters et al. (2010) performed a comprehensive study of the region by combining current and wind data with an unstructured grid model, including accurate topography to examine the leading mechanisms across Greater Cook Strait. By running their model with, and without, several of the important forcing factors, they were able to estimate the significance of these factors in different areas. The model of Walters et al. (2010) shows flow separation at the northern edge of Cook Strait forced by the eastward flux through the gap with their Fig. 7 showing residual currents along the northern side of Cook Strait, just to the west of Cape Palliser and Palliser Bay. As the flow passes Baring Head, the surface velocities intensify and the current detaches. A recirculating current can be seen on the downstream side of the head, showing that flow separation occurs here.

One of the most striking observed features in the area is a large warm-core eddy to the east of the strait, as shown in Fig. 7a [from Barnes (1985)]. This eddy appears to be a stable feature, fixed in position even though there is no obvious explanatory bathymetric feature. The origin of this eddy and the reason for its apparent stability are not known, but it is suggested here that the eddy is formed as the current through the strait separates at Cape Palliser, on the northern edge of the gap.

The volumetric flux through the strait is approximately 0.6 Sv that dominate the residual currents, although tidal stresses are also important around headlands. The currents concentrate on the northern side as they pass through the strait. The Cook Strait is thus modeled

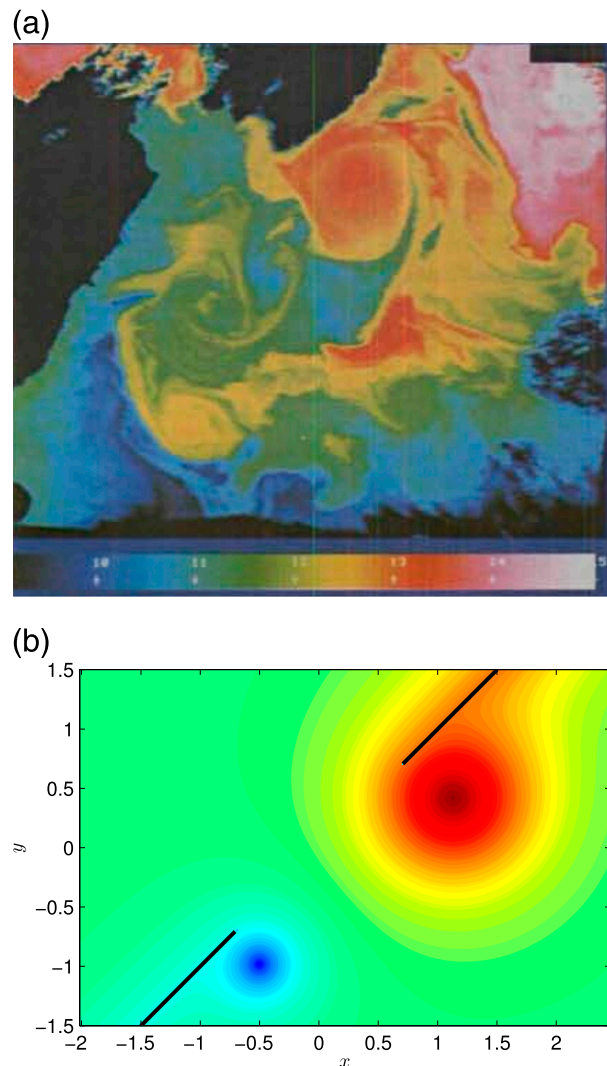


FIG. 7. (a) Sea surface temperature in the vicinity of the Cook Strait reproduced from Barnes (1985). (b) The surface perturbation for QGBM vortices shed from the edges of a gap for $a = 0.4$ at time $t = 4$ in the simulation. There is unit flux along the upper wall and flux of $1/3$ along the lower wall.

here as a gap in a wall representing the North and South Islands with a flux through the gap of strength $Q_2 + Q_1$, where Q_1 is the flux northward up the west coast of the South Island and Q_2 is the flux southward down the west coast of the North Island, given by applying the boundary conditions $\eta = Q_1$ on the lower wall, $\eta = Q_2$ on the upper wall, and $\eta \rightarrow 0$ at infinity. The strengthening of the current on the northern side of the strait is modeled by taking $Q_1 < Q_2$. Here, the parameter $a = L_r/L$ is the ratio of the Rossby radius L_r to the gap half-width L . Two sheddies are formed: one from either edge of the gap. The streamfunction can be computed numerically using the spectral method described in Southwick et al. (2015) and the mapping

$$z = \cosh Z, \quad (13)$$

which takes the strip $0 < Y < \pi$ in the computational domain (coordinates $Z = X + iY$) to the physical domain (coordinates $z = x + iy$) with the top and bottom boundaries of the strip mapping to the left and right walls, respectively.

The width of the gap where the eddy is formed is approximately 125 km, and the Rossby radius is around 25 km (Chelton et al. 1998), giving $a = 0.4$. Figure 7b shows the surface height from a simulation with this value of a ; $Q_2 = 1$ and $Q_1 = 1/3$ at time $t = 4$. Two shed eddies of opposite-signed circulations are clearly visible with a much larger eddy on the northern edge of the strait, appearing similar to the observations in Fig. 7a. After an initial period, QGBM vortices grow slowly, particularly when a is small (Southwick et al. 2015). This slow growth could be an explanation for the unchanging position of the observed Cook Strait eddy.

This eddy formation mechanism could cause eddies to form anywhere where there is significant flow through a gap. In many places the dynamics are complicated, however, by other factors such as significant differences in important properties such as sea surface height, ocean depth, or salinity across the gap. These differences can also provide a mechanism for the formation of eddies such as Mediterranean outflow eddies “meddies” (Serra et al. 2005) and Indonesian Throughflow eddies “teddies” (Nof et al. 2002), where significant potential vorticity differences due to the stretching of vortex columns may dominate the dynamics (Southwick et al. 2016, manuscript submitted to *J. Phys. Oceanogr.*; E. R. Johnson et al. 2016, unpublished manuscript).

b. Eddies encountering gaps: The interaction of North Brazil Current rings with the Lesser Antilles

There are many examples of eddies encountering either single gaps in topography, such as Caribbean cyclones entering the Yucatan Channel (Richardson 2005), or multiple gaps, such as meddies encountering an underwater ridge (Dewar 2002) with the eddy trajectory differing significantly depending on whether it passes through or across the gap. The dynamics of this process is sensitive to the details of the local topography and bathymetry and, as these details may not be sufficiently resolved in large-scale ocean models, have been the focus of much attention.

A particularly important example concerns the fate of the NBC rings. As the NBC retroflects, large eddies (known as the NBC rings) are periodically shed at the rate of $6\text{--}9\text{ yr}^{-1}$ with each eddy carrying a flux of around 1 Sv (Goni and Johns 2001). The large size of the NBC rings and their shedding frequency represents a

significant transport mechanism of warm South Atlantic surface water into the Northern Hemisphere. They travel northwest until they meet the island chain of the Lesser Antilles that blocks their path.

Whether the NBC rings pass through gaps between the Lesser Antilles, disintegrate upon collision with the islands, or continue northward past them is of key interest. Some observations suggest that they rarely pass through the southern Lesser Antilles intact (Johns et al. 2003) but that in many cases they may disintegrate with their mass passing through the gaps and into the Caribbean sea (Fratantoni and Richardson 2006; Fratantoni and Glickson 2002). It may be possible for NBC rings to enter through the northern Lesser Antilles as “quasi-coherent” structures (Cruz Gómez and Bulgakov 2007). Additionally, drifter studies suggest that anticyclones to the west of the Lesser Antilles may be formed from the NBC ring anticyclonic vorticity (Richardson 2005). However, in some numerical simulations (Garraffo et al. 2003), the NBC rings enter the Caribbean nearly intact.

Simmons and Nof (2002) present an analytical model and numerical results that suggest that weak eddies are able to squeeze through the gaps but intense eddies resist. The circulation around the islands in their numerical experiments increased due to flow separation at the island edges, which has also been observed in experimental investigations. Duran-Matute and Velasco Fuentes (2008) performed experiments on an eddy encountering a gap and observed eddies formed by flow separation interacting with the incident eddy. This caused a looping trajectory, differing from their otherwise effective point vortex theory, as shown in Fig. 8a, which combines their Figs. 13 and 14. Tanabe and Cenedese (2008) also observed eddies forming from separated flow in the lee of the islands in their experiments, which investigated an eddy passing a chain of circular islands.

Point vortex models of eddies approaching a gap have been useful in understanding the dynamics of the situation and give precise criteria for whether an eddy will pass through or leap over a gap, depending on the background flow and the eddy’s initial distance from the wall (Johnson and McDonald 2005; Nilawar et al. 2012). These models do not, however, allow flow separation. This section reconsiders a point vortex encountering a gap in a wall, modeling flow separation with the QGBM model.

Consider first the situation with no background flow ($\eta = 0$ on the walls, $\eta \rightarrow 0$ far from the walls) and a point vortex approaching the gap from an initial position (x_0, y_0) , where $x_0 \gg a$ and the initial distance from the wall y_0 is varied. In the absence of flow separation, there is a

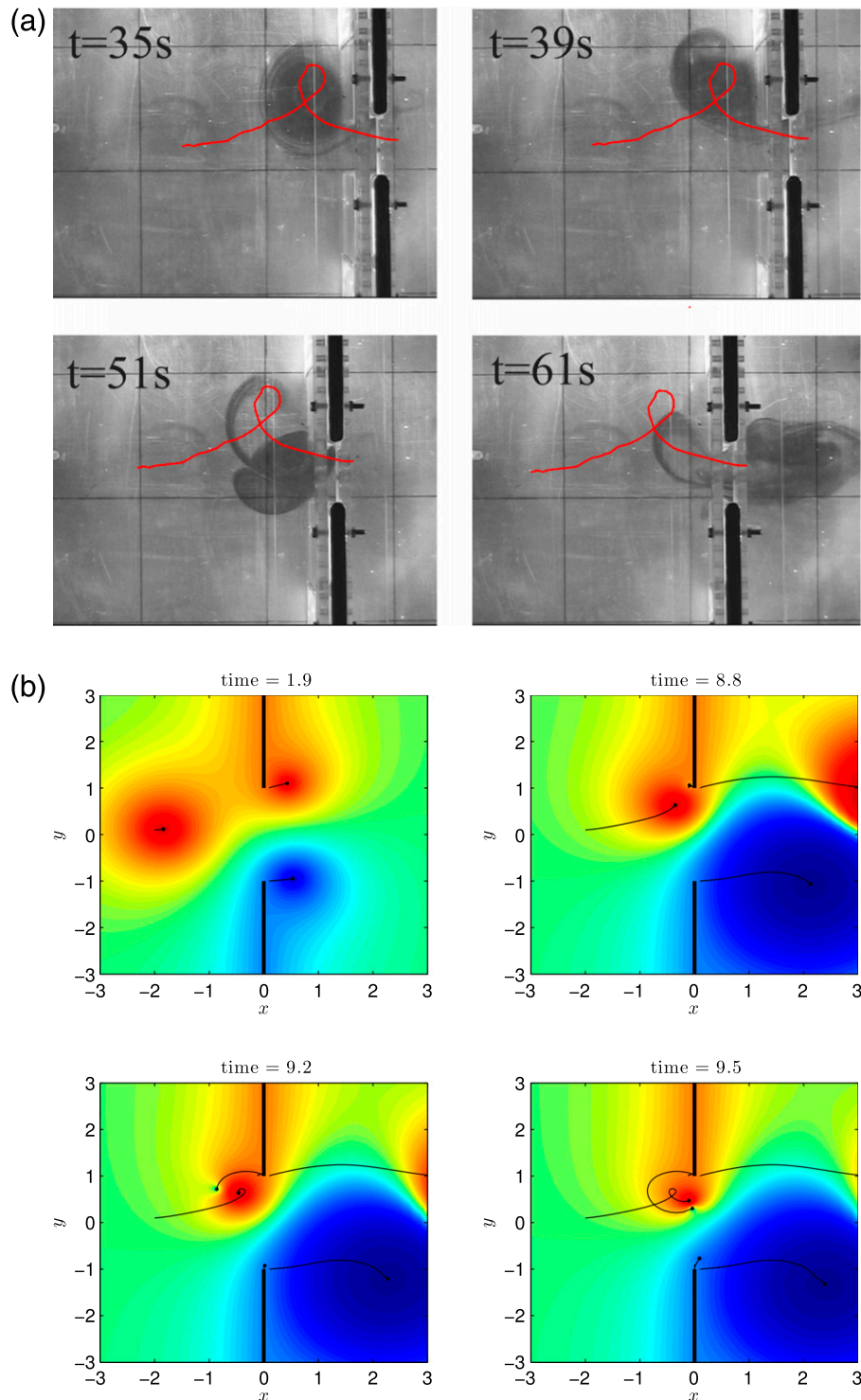


FIG. 8. (a) The evolution of an intense vortex marked with dye being driven through gap in a wall by a current in a rotating tank experiment reproduced from [Duran-Matute and Velasco Fuentes \(2008\)](#). The red line shows the trajectory of the center of the incident vortex. (b) The surface perturbation and vortex trajectories (black lines) for a simulation of a vortex being driven through a gap by a current in a similar arrangement to [Fig. 8a](#). The incident vortex has strength $\Gamma = 10$ and $a = 1$, and the flux through the gap is $Q = 2$.

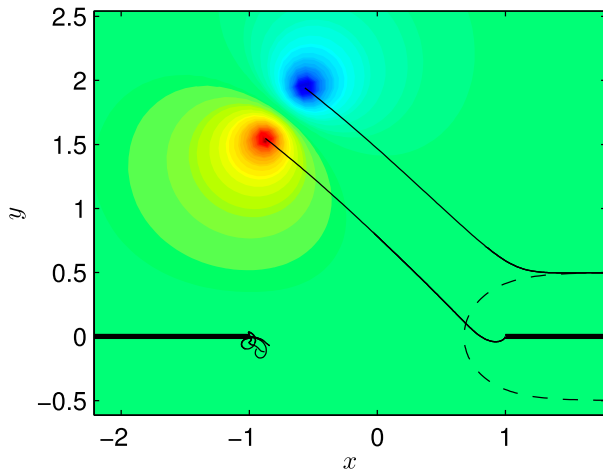


FIG. 9. Vortex trajectories for an incident vortex with no background flow without shedding (dashed line) and with shedding (solid lines). The color shows the surface perturbation at the final time in the simulation with shedding. The incident vortex is initially a distance of $1/2$ from the wall and $a = 1$.

critical value of y_0 , depending on a , above which vortices leap the gap, and below which they pass through. When flow separation is included, very different results are found. For no values of y_0 or a does the vortex pass through the gap. A typical scenario where, in the absence of shedding, a vortex would have passed through is shown in Fig. 9. Here, the sheddy from the near wall pairs with the incident vortex and prevents it from entering the gap with the pair ultimately propagating away. Very little vorticity is generated at the far tip. The result that vortices can no longer self-advect through a gap relates to those of Southwick et al. (2015), who consider a similar situation with a single plate instead of a gap. They found that, for all a , the incident vortex and shed vortex paired up and moved away in the upper half plane without rounding the plate tip.

The NBC rings are aided in passing through gaps by the presence of a background flow. Considering the previous scenario, but with an additional unidirectional flow through the gap of flux Q , achieved with the conditions $\eta = Q/2$ on the left wall, $\eta = -Q/2$ on the right, and $\eta \rightarrow 0$ far from the walls, shows that for flux Q above a certain critical value the current overpowers the resistance of the vortex and advects it through the gap. Typically a current of flux $Q = 0.2$ was able to overpower a vortex with unit circulation. This example is shown in Fig. 10. Here, a significant amount of vorticity is generated from both edges of the gap driven by the unidirectional background current.

The experiments of Duran-Matute and Velasco Fuentes (2008) offer a good test of the QGBM method in this single-gap geometry. They found good agreement

between point vortex methods and their experiments until the generation of vorticity at the walls became significant. Figure 8a shows the results of one of their experiments for a more intense vortex (combining their Figs. 13 and 14). As the incident vortex approaches the gap, vorticity is shed from the nearest edge. This shed vortex pairs up with the incident vortex and they perform one spiral before passing through the gap. The red line shows the trajectory of the center of the incident vortex that is visualized with dye in the experiment.

The results of a QGBM simulation with the incident vortex starting at $(x_0, y_0) = (-2, 0)$, with $\Gamma = 10$, $a = 1$, and $Q = 2$ are shown in Fig. 8b. The coloring in Fig. 8b indicates the surface perturbation and so is not directly comparable with the dye in Fig. 8a. In Fig. 8b, the incoming vortex induces the separation and formation of a sheddy of oppositely signed vorticity on the upper wall. The two vortices pair and perform a single loop before passing through the gap, similar to the behavior observed in the experiments. The simulations in Fig. 8b are typical, with this behavior appearing to be robust across a range of parameters. In the simulation, the throughflow also generates eddies at both edges of the gap. As there was no dye injected in these regions in the experiment, it does not appear possible to decide whether these vortices were present in the experiments. The QGBM model captures the key feature of these experiments, the looping trajectory, where classic point vortex methods cannot and suggests that separation can significantly affect eddy trajectories near topography. The effect of the separated shear layer may help explain the reluctance of the NBC rings to pass through gaps and the large number of eddies observed to the west of the islands.

c. Unidirectional flow through a gap: The Canary Eddy Corridor

The Canary Current is a wind-driven eastern boundary current flowing southwestward along the western coast of Africa as far as Senegal. Sheddies are generated continually in the lee of the Canary Islands, which form a partial barrier across the current (Sangrà et al. 2007; Barton 2001). Figure 3 of Barton (2001) shows multiple sheddies visible in the sea surface temperature and his Fig. 4 shows the looping profile of a drifter trapped in a sheddy. These eddies form a long chain known as the Canary Eddy Corridor (Sangrà et al. 2009) and may form the origin for swesties (shallow subtropical subducting westward-propagating eddies; Pingree 1996).

Here, sheddies formed in the wakes of gaps between islands are modeled. Consider a single gap in a wall with a symmetric, unidirectional current of flux Q

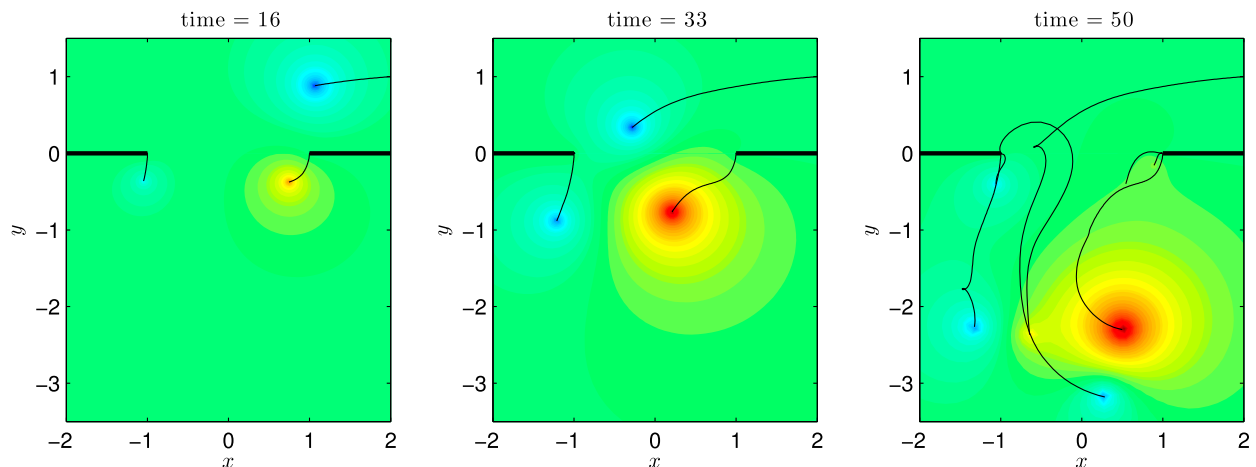


FIG. 10. Vortex trajectories for an incident vortex with a background flow of strength $Q = 0.2$. The color shows the surface perturbation at the final time in the simulation. The parameter $a = 1$ and the incident vortex is initially a distance $y_0 = 1/2$ from the wall.

through the gap, given by setting $\eta = -Q/2$ on the right wall, $\eta = Q/2$ on the left wall, and $\eta \rightarrow 0$ at large distances.

The original Brown–Michael model has no mechanism for curtailing the growth of a sheddy; as the separated shear layer rolls up, the eddy grows monotonically and typically drifts downstream. In real flows, as the eddy grows, factors like instabilities in the shear layer become more important and eventually destroy the vortex sheet, stopping the growth of the sheddy and freeing the shear layer to roll up into a new shed eddy. To represent this process, a new condition determining when a sheddy stops growing and a new sheddy forms is introduced in this section.

For outflows, shed vortices tend to form pairs (Blondeaux and De Bernardinis 1983). Thus, one appropriate choice of termination condition is to halt the growth of an eddy when the distance between the vortex and the separation point, an estimate of the length of the vortex sheet, is longer than the distance to the nearest vortex. The eddies then form a pair with their circulations fixed and move away freely with new sheddies forming at the gap.

Figure 11 shows a simulation with this condition: $a = 1$ and a unidirectional background current through the gap of flux $Q = 1$. Vortex pairs are shed regularly and periodically with a shedding frequency of approximately 0.2 (eight eddies are formed over a timespan of length 40), giving a Strouhal number (defined as $S_t = nL/U$ for shedding frequency n , length scale $L = a$, and velocity scale $U = 1/a$) of $S_t \approx 0.2$. This value is consistent with the results of Dong et al. (2007), showing that three-dimensional, stratified, rotating flow has a similar Strouhal number to the classic von Kármán vortex street

for nonrotating, nonstratified, two-dimensional flow past an object, perhaps hinting that the underlying dynamics are controlled by the vortex shedding. The first four panels of Fig. 11 show the evolution of a pair of sheddies over their formation period up to the point where their feeding vortex sheets have collapsed and a new pair of sheddies have started growing. The fifth panel gives a larger-scale view over longer time to show the periodic shedding.

The Rossby radius around the Canary Islands is approximately 25 km (Chelton et al. 1998), the islands are a similar size to the Rossby radius, and a typical Canary Current speed is 0.05 m s^{-1} . With these scalings, the QGBM model shows that the vortices grow to their maximum strength over a period of approximately 50 days, giving 14 eddies shed per year, a similar figure to the 17 eddies shed on average per year observed by Sangrà et al. (2009). The fully developed eddies have velocities in the range $0.5\text{--}2 \text{ m s}^{-1}$ between a third and a whole Rossby radius from the eddy center, larger than, but comparable with, the velocities of around 0.5 m s^{-1} observed by Sangrà et al. (2007).

Although these criteria give realistic results, other choices are possible. An alternative would be to set a maximum feasible circulation for the vortex Γ_{\max} . Varying Γ_{\max} gives a continuum of models with the original Brown–Michael corresponding to $\Gamma_{\max} \rightarrow \infty$, and a vortex sheet model given by $\Gamma_{\max} \rightarrow 0$. Figures 12 and 13 show examples using $\Gamma_{\max} = 2$ and $\Gamma_{\max} = 25$ with $a = 1$ and $Q = 1$. In both cases many sheddies are generated. For $\Gamma_{\max} = 2$, the growing sheddy is frequently pulled back toward the separation point by another eddy, causing its circulation to decrease and a new sheddy to form and leading to the generation of a large

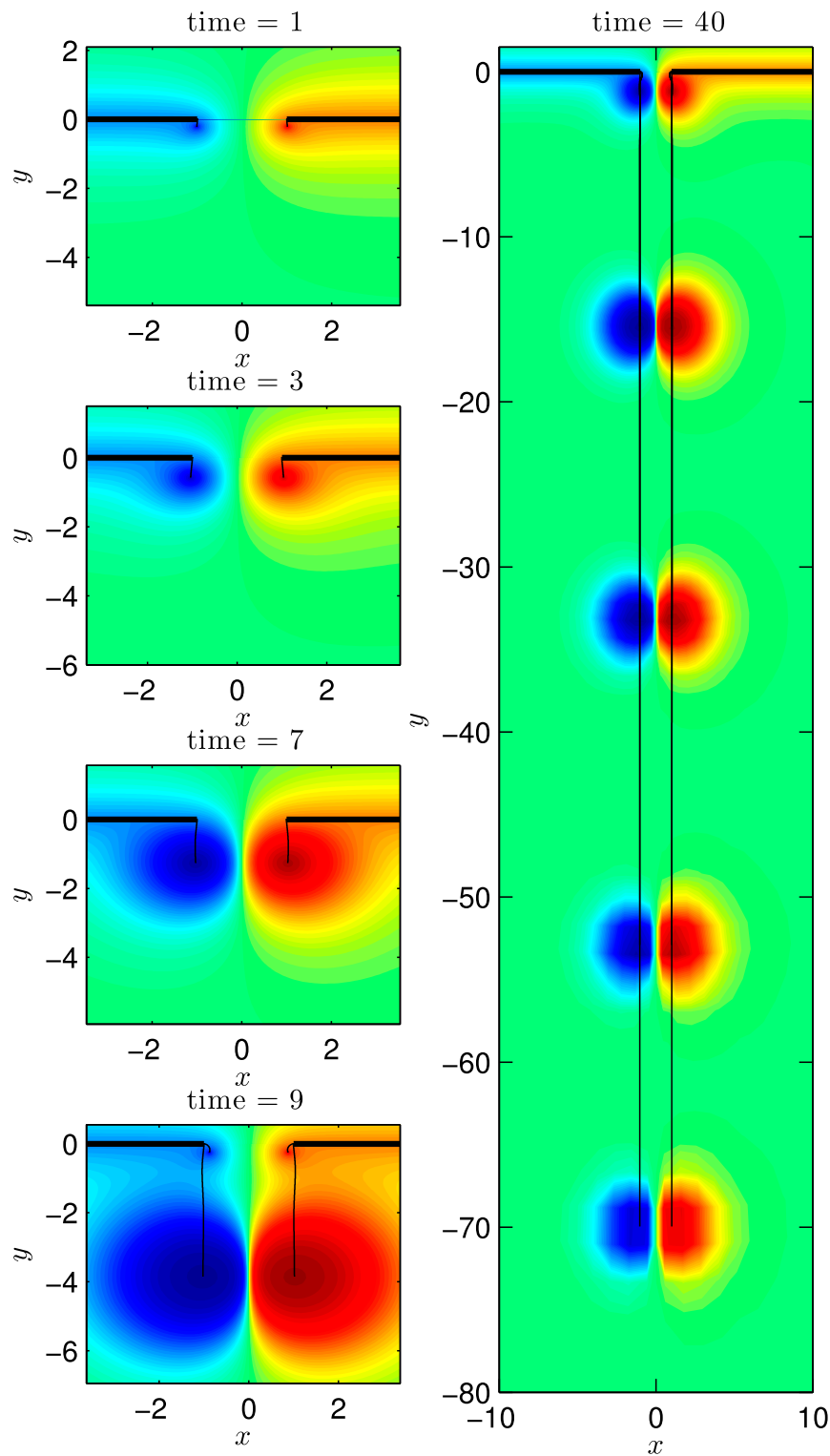


FIG. 11. The surface perturbation from a QGBM simulation of a current through a gap of flux $Q = 1$ driving the formation of shed eddies for $a = 1$. The four snapshots on the left span the growth period of a pair of sheddies from their genesis until they are set free and new sheddies begin to form. The panel on the right shows a larger-scale view after a longer period of time to show the periodic behavior. The trajectories of the centers of the eddies are marked as black lines.

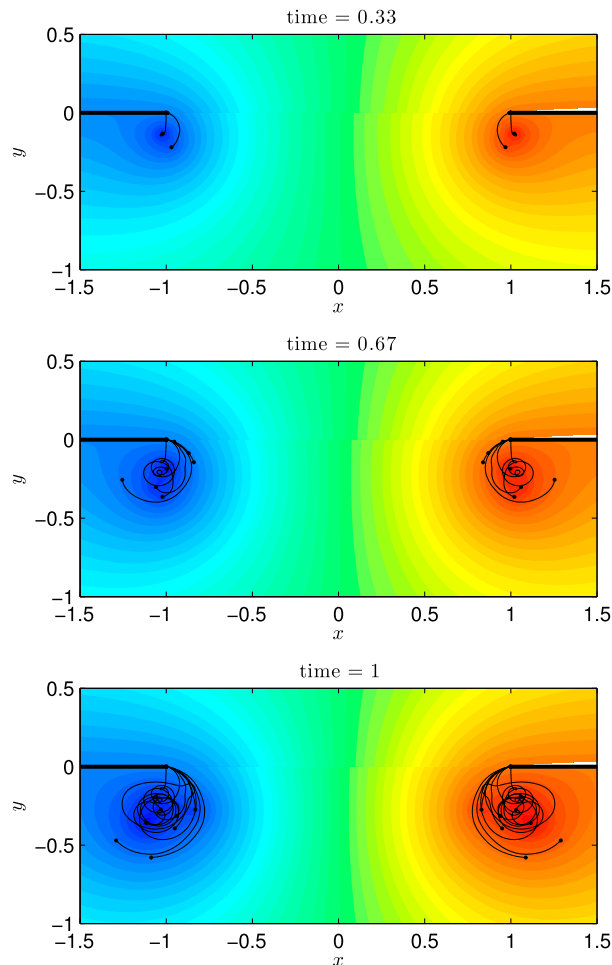


FIG. 12. The surface perturbation and sheddy trajectories (black lines) at three points in time from a simulation of sheddies formed from a current of flux $Q = 1$ passing through a gap for $a = 1$ and with the condition that the magnitude of the sheddy circulation cannot exceed $\Gamma_{\max} = 2$.

number of vortices, some of which have very small circulations. These many smaller eddies concentrate into an area resembling a single larger eddy in a process similar to the rolling up of the vortex sheet into a single, coherent eddy seen in Figs. 1 and 2.

The $\Gamma_{\max} = 25$ condition gives dynamics somewhere between the clustered, many vortex shedding of $\Gamma_{\max} = 2$ (Fig. 12) and the regular periodic shedding of the condition on the vortex sheet lengths (Fig. 11). Several distinct, strong sheddies are formed, but these are close enough that the nonlinear interactions between them cause complex spiral trajectories and leapfrogging of eddies past eddies shed at earlier times.

Although the results of the simulation of Fig. 12 appear significantly different from those of Fig. 11, the center of vorticity follows a very similar path for

small and moderate times. A many vortex simulation like this becomes more computationally intensive as the number of vortices grows and is significantly more difficult to interpret than a standard Brown–Michael simulation. Using a condition such as $\Gamma_{\max} = 2$ sacrifices some of the key advantages of the QGBM method.

6. Conclusions

Recent work showing that vertical eddy diffusivity causes a horizontal shear layer to form at sloped ocean margins has clarified the mechanism for the formation of sheddies and suggests that small-scale viscous separation is underrepresented in ocean models. Models without sufficient resolution, sloping boundaries, and viscous boundary conditions fail to capture this thin shear layer, its detachment, and subsequent dynamical effects.

Detached shear layers typically roll up into concentrated spirals of vorticity and form or behave as large, coherent eddies. This paper models the formation of these mesoscale eddies and their impact in a number of oceanographic contexts using a simple approach based on the Brown–Michael model of vortex shedding, adapted for quasigeostrophic oceanographic flows. The simple nature of the model means it is straightforward to implement, simple to diagnose, and that it highlights the key physical processes. The aim is to show that an inviscid model with explicit representations of the important vortical features can accurately represent observed features of oceanic flows while avoiding many of the difficulties of viscous models associated with the very high resolution required to resolve thin but important boundary layers.

The model has been applied to observations, numerical experiments, and experimental results in a number of oceanographic situations: the Canary Eddy Corridor, Agulhas cyclones, Cook Strait Throughflow, California Current at Point Sur, and the collision of the North Brazil Current rings with the Lesser Antilles. Comparison between sea surface height data showing the formation of an Agulhas cyclone and the results of a QGBM simulation suggests that the model captures the growth of the shed eddy. Rotating tank experiments investigating a vortex advected through a gap show trajectories significantly affected by flow separation as a shed eddy pairs with the vortex and causes a looping trajectory, a result reproduced by the QGBM model.

Nonseparating point vortex models of the North Brazil Current rings colliding with the Lesser Antilles do not capture the reluctance of these rings to pass

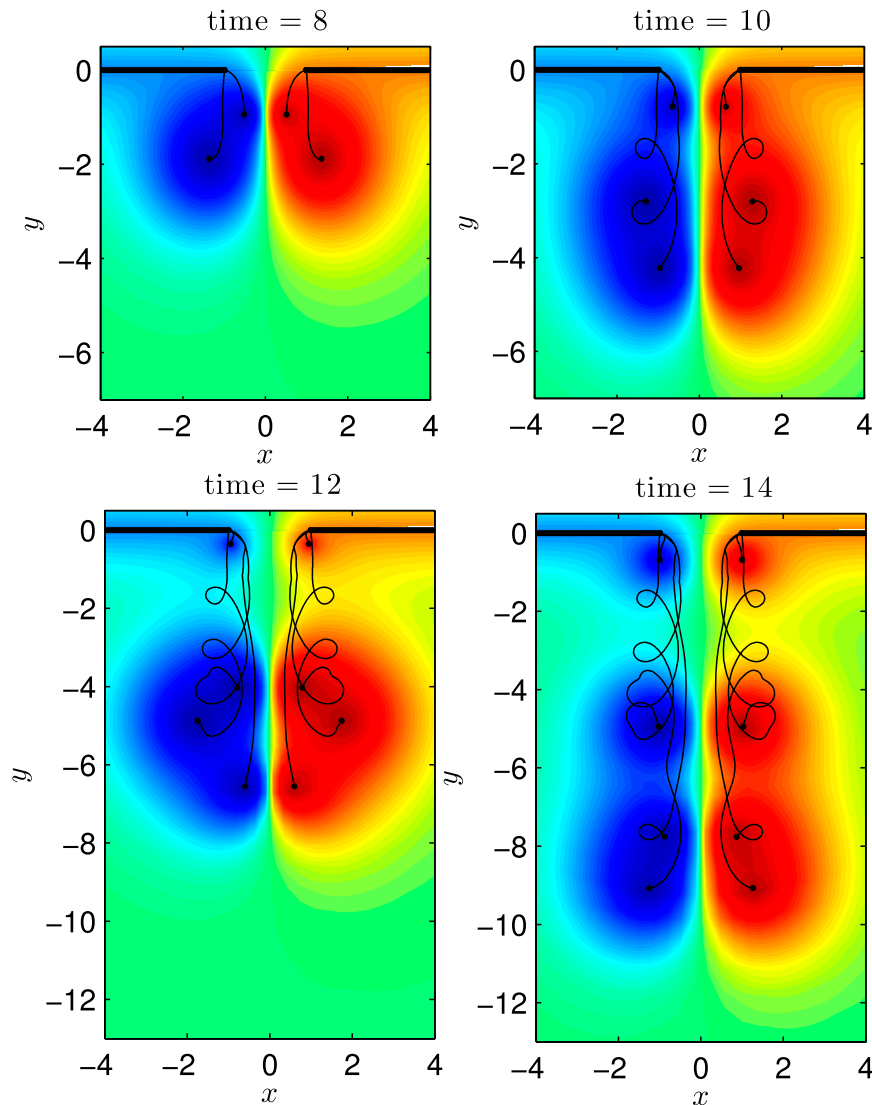


FIG. 13. The surface perturbation and sheddy trajectories (black lines) at four points in time from a simulation of sheddies formed from a current of flux $Q = 1$ passing through a gap for $a = 1$ and with the condition that the magnitude of the sheddy circulation cannot exceed $\Gamma_{\max} = 25$.

between island gaps. The QGBM model, which allows flow separation, shows that eddies are far less likely to pass through the island gaps. The vorticity expelled by flow separation may thus be an important reason why North Brazil Current rings do not often enter the Caribbean intact.

The QGBM model principally aims to understand the formation of sheddies in the ocean through qualitative representations of the key dynamics. Although it is not intended to make quantitative calculations, the model appears to predict key eddy properties such as current speeds, surface deformations, and the formation period of the sheddies of the same order of

magnitude to those observed and given by numerical simulations. The model here is based on quasigeostrophic flow, an appropriate first model for the dynamics of sheddies in many cases, which enables cheap and quick investigation of flows. However, effects such as outcropping of isopycnals, continuous stratification, and bathymetry may be important in particular applications, and more detailed models may be more appropriate. A potential extension of the present model would be to use a rotating shallow-water model, enabling the inclusion of other influencing effects but sacrificing some of the simplicity and speed offered by the QGBM approach.

Acknowledgments. O.R.S. was supported by an EPSRC DTA studentship (Grant EP/J500331/1).

REFERENCES

- Barnes, E. J., 1985: Eastern Cook Strait region circulation inferred from satellite-derived, sea-surface, temperature data. *N. Z. J. Mar. Freshwater Res.*, **19**, 405–411, doi:10.1080/00288330.1985.9516105.
- Barton, E. D., 2001: Island wakes. Encyclopedia of Ocean Sciences, Academic Press, 1397–1403, doi:10.1006/rwos.2001.0140.
- Blondeaux, P., and B. De Bernardinis, 1983: On the formation of vortex pairs near orifices. *J. Fluid Mech.*, **135**, 111–122, doi:10.1017/S0022112083002980.
- Boebel, O., J. Lutjeharms, C. Schmid, W. Zenk, T. Rossby, and C. Barron, 2003: The Cape Cauldron: A regime of turbulent inter-ocean exchange. *Deep-Sea Res. II*, **50**, 57–86, doi:10.1016/S0967-0645(02)00379-X.
- Boyer, D. L., and L. Tao, 1987: On the motion of linearly stratified rotating fluids past capes. *J. Fluid Mech.*, **180**, 429–449, doi:10.1017/S0022112087001885.
- Brown, C. E., and W. H. Michael Jr., 1954: Effect of leading-edge separation on the lift of a delta wing. *J. Aeronaut. Sci.*, **21**, 690–694.
- Chelton, D. B., R. A. DeSzoeke, M. G. Schlax, K. El Naggar, and N. Siwertz, 1998: Geographical variability of the first baroclinic Rossby radius of deformation. *J. Phys. Oceanogr.*, **28**, 433–460, doi:10.1175/1520-0485(1998)028<0433:GVOTFB>2.0.CO;2.
- Chou, K.-H., and C.-C. Wu, 2008: Typhoon initialization in a mesoscale model combination of the bogus vortex and the dropwindsonde data in DOTSTAR. *Mon. Wea. Rev.*, **136**, 865–879, doi:10.1175/2007MWR2141.1.
- Collins, C., N. Garfield, T. Rago, F. Rischmiller, and E. Carter, 2000: Mean structure of the inshore countercurrent and California Undercurrent off Point Sur, California. *Deep-Sea Res. II*, **47**, 765–782, doi:10.1016/S0967-0645(99)00126-5.
- Cortelezzi, L., and A. Leonard, 1993: Point vortex model of the unsteady separated flow past a semi-infinite plate with transverse motion. *Fluid Dyn. Res.*, **11**, 263–295, doi:10.1016/0169-5983(93)90013-Z.
- Cruz Gómez, R. C., and S. N. Bulgakov, 2007: Remote sensing observations of the coherent and non-coherent ring structures in the vicinity of Lesser Antilles. *Ann. Geophys.*, **25**, 331–340, doi:10.5194/angeo-25-331-2007.
- Davey, M., R. Hurst, and E. Johnson, 1993: Topographic eddies in multilayer flow. *Dyn. Atmos. Oceans*, **18**, 1–27, doi:10.1016/0377-0265(93)90002-O.
- Dewar, W. K., 2002: Baroclinic eddy interaction with isolated topography. *J. Phys. Oceanogr.*, **32**, 2789–2805, doi:10.1175/1520-0485(2002)032<2789:BEIWT>2.0.CO;2.
- , J. C. McWilliams, and M. J. Molemaker, 2015: Centrifugal instability and mixing in the California Undercurrent. *J. Phys. Oceanogr.*, **45**, 1224–1241, doi:10.1175/JPO-D-13-0269.1.
- Dong, C., J. C. McWilliams, and A. F. Shchepetkin, 2007: Island wakes in deep water. *J. Phys. Oceanogr.*, **37**, 962–981, doi:10.1175/JPO3047.1.
- Duran-Matute, M., and O. U. Velasco Fuentes, 2008: Passage of a barotropic vortex through a gap. *J. Phys. Oceanogr.*, **38**, 2817–2831, doi:10.1175/2008JPO3887.1.
- Eldredge, J., and C. Wang, 2010: High-fidelity simulations and low-order modeling of a rapidly pitching plate. *Proc. 40th Fluid Dynamics Conf. and Exhibit*, AIAA Paper 2010-4281, Chicago, IL, AIAA, 1–19.
- Fratantoni, D. M., and D. A. Glickson, 2002: North Brazil Current ring generation and evolution observed with SeaWiFS. *J. Phys. Oceanogr.*, **32**, 1058–1074, doi:10.1175/1520-0485(2002)032<1058:NBCRGA>2.0.CO;2.
- , and P. L. Richardson, 2006: The evolution and demise of North Brazil Current rings. *J. Phys. Oceanogr.*, **36**, 1241–1264, doi:10.1175/JPO2907.1.
- Garraffo, Z. D., W. Johns, E. Chassignet, and G. Goni, 2003: North Brazil Current rings and transport of southern waters in a high resolution numerical simulation of the North Atlantic. *Interhemispheric Water Exchange in the Atlantic Ocean*, G. J. Goni and P. Malanotte-Rizzoli, Eds., Elsevier Oceanography Series, Vol. 68, Elsevier, 375–409, doi:10.1016/S0422-9894(03)80155-1.
- Goni, G. J., and W. E. Johns, 2001: A census of North Brazil Current rings observed from TOPEX/POSEIDON altimetry: 1992–1998. *Geophys. Res. Lett.*, **28**, 1–4, doi:10.1029/2000GL011717.
- Graham, J. M. R., 1980: The forces on sharp-edged cylinders in oscillatory flow at low Keulegan–Carpenter numbers. *J. Fluid Mech.*, **97**, 331–346, doi:10.1017/S0022112080002595.
- , 1983: The lift on an aerofoil in starting flow. *J. Fluid Mech.*, **133**, 413–425, doi:10.1017/S0022112083001986.
- Gula, J., M. J. Molemaker, and J. C. McWilliams, 2015: Topographic vorticity generation, submesoscale instability and vortex street formation in the Gulf Stream. *Geophys. Res. Lett.*, **42**, 4054–4062, doi:10.1002/2015GL063731.
- Heywood, K. J., D. P. Stevens, and G. R. Bigg, 1996: Eddy formation behind the tropical island of Aldabra. *Deep-Sea Res. I*, **43**, 555–578, doi:10.1016/0967-0637(96)00097-0.
- Hogg, N. G., and H. M. Stommel, 1985: The heton, an elementary interaction between discrete baroclinic geostrophic vortices, and its implications concerning eddy heat-flow. *Proc. Roy. Soc. London*, **A397**, 1–20, doi:10.1098/rspa.1985.0001.
- Hsiao, L.-F., C.-S. Liou, T.-C. Yeh, Y.-R. Guo, D.-S. Chen, K.-N. Huang, C.-T. Terng, and J.-H. Chen, 2010: A vortex relocation scheme for tropical cyclone initialization in Advanced Research WRF. *Mon. Wea. Rev.*, **138**, 3298–3315, doi:10.1175/2010MWR3275.1.
- Isoguchi, O., M. Shimada, F. Sakaida, and H. Kawamura, 2009: Investigation of Kuroshio-induced cold-core eddy trains in the lee of the Izu Islands using high-resolution satellite images and numerical simulations. *Remote Sens. Environ.*, **113**, 1912–1925, doi:10.1016/j.rse.2009.04.017.
- Jiang, M., M. Zhou, S. P. Libby, and D. M. Anderson, 2011: Dynamics of a mesoscale eddy off Cape Ann, Massachusetts in May 2005. *Deep-Sea Res. I*, **58**, 1130–1146, doi:10.1016/j.dsr.2011.08.009.
- Johns, W. E., R. J. Zantopp, and G. Goni, 2003: Cross-gyre transport by North Brazil Current rings. *Interhemispheric Water Exchange in the Atlantic Ocean*, G. J. Goni and P. Malanotte-Rizzoli, Eds., Elsevier Oceanography Series, Vol. 68, Elsevier, 411–441, doi:10.1016/S0422-9894(03)80156-3.
- Johnson, E. R., and N. R. McDonald, 2005: Vortices near barriers with multiple gaps. *J. Fluid Mech.*, **531**, 335–358, doi:10.1017/S0022112005003976.
- Klinger, B. A., 1994: Baroclinic eddy generation at a sharp corner in a rotating system. *J. Geophys. Res.*, **99**, 12515–12531, doi:10.1029/93JC03585.
- Kurihara, Y., M. A. Bender, and R. J. Ross, 1993: An initialization scheme of hurricane models by vortex specification. *Mon.*

- Wea. Rev.*, **121**, 2030–2045, doi:[10.1175/1520-0493\(1993\)121<2030:AISSOHM>2.0.CO;2](https://doi.org/10.1175/1520-0493(1993)121<2030:AISSOHM>2.0.CO;2).
- , —, R. E. Tuleya, and R. J. Ross, 1995: Improvements in the GFDL hurricane prediction system. *Mon. Wea. Rev.*, **123**, 2791–2801, doi:[10.1175/1520-0493\(1995\)123<2791:IIITGHP>2.0.CO;2](https://doi.org/10.1175/1520-0493(1995)123<2791:IIITGHP>2.0.CO;2).
- Lutjeharms, J. R. E., O. Boebel, and H. T. Rossby, 2003: Agulhas cyclones. *Deep-Sea Res. II*, **50**, 13–34, doi:[10.1016/S0967-0645\(02\)00378-8](https://doi.org/10.1016/S0967-0645(02)00378-8).
- Manela, A., and L. Huang, 2013: Point vortex model for prediction of sound generated by a wing with flap interacting with a passing vortex. *J. Acoust. Soc. Amer.*, **133**, 1934–1944, doi:[10.1121/1.4792246](https://doi.org/10.1121/1.4792246).
- Michelin, S., and S. G. Llewellyn Smith, 2010: Falling cards and flapping flags: Understanding fluid solid interactions using an unsteady point vortex model. *Theor. Comput. Fluid Dyn.*, **24**, 195–200, doi:[10.1007/s00162-009-0117-6](https://doi.org/10.1007/s00162-009-0117-6).
- Molemaker, M. J., J. C. McWilliams, and W. K. Dewar, 2015: Submesoscale instability and generation of mesoscale anticyclones near a separation of the California Undercurrent. *J. Phys. Oceanogr.*, **45**, 613–629, doi:[10.1175/JPO-D-13-0225.1](https://doi.org/10.1175/JPO-D-13-0225.1).
- Nilawar, R. S., E. R. Johnson, and N. R. McDonald, 2012: Finite Rossby radius effects on vortex motion near a gap. *Phys. Fluids*, **24**, 066601, doi:[10.1063/1.4721432](https://doi.org/10.1063/1.4721432).
- Nof, D., T. Pichevin, and J. Sprintall, 2002: “Teddies” and the origin of the Leeuwin Current. *J. Phys. Oceanogr.*, **32**, 2571–2588, doi:[10.1175/1520-0485-32.9.2571](https://doi.org/10.1175/1520-0485-32.9.2571).
- Pedrizzetti, G., 2010: Vortex formation out of two-dimensional orifices. *J. Fluid Mech.*, **655**, 198–216, doi:[10.1017/S0022112010000844](https://doi.org/10.1017/S0022112010000844).
- Penven, P., J. R. E. Lutjeharms, P. Marchesiello, C. Roy, and S. J. Weeks, 2001: Generation of cyclonic eddies by the Agulhas Current in the lee of the Agulhas Bank. *Geophys. Res. Lett.*, **28**, 1055–1058, doi:[10.1029/2000GL011760](https://doi.org/10.1029/2000GL011760).
- Pingree, R. D., 1996: A shallow subtropical subducting westward propagating eddy (Swesty). *Philos. Trans. Roy. Soc. London*, **A354**, 979–1026, doi:[10.1098/rsta.1996.0039](https://doi.org/10.1098/rsta.1996.0039).
- Richardson, P., 2005: Caribbean Current and eddies as observed by surface drifters. *Deep-Sea Res. II*, **52**, 429–463, doi:[10.1016/j.dsr2.2004.11.001](https://doi.org/10.1016/j.dsr2.2004.11.001).
- Rott, N., 1956: Diffraction of a weak shock with vortex generation. *J. Fluid Mech.*, **1**, 111–128, doi:[10.1017/S0022112056000081](https://doi.org/10.1017/S0022112056000081).
- Sangrà, P., and Coauthors, 2007: On the nature of oceanic eddies shed by the Island of Gran Canaria. *Deep-Sea Res. I*, **54**, 687–709, doi:[10.1016/j.dsr.2007.02.004](https://doi.org/10.1016/j.dsr.2007.02.004).
- , and Coauthors, 2009: The Canary Eddy Corridor: A major pathway for long-lived eddies in the subtropical North Atlantic. *Deep-Sea Res. I*, **56**, 2100–2114, doi:[10.1016/j.dsr.2009.08.008](https://doi.org/10.1016/j.dsr.2009.08.008).
- Serra, N., I. Ambar, and R. H. Käse, 2005: Observations and numerical modelling of the Mediterranean outflow splitting and eddy generation. *Deep-Sea Res. II*, **52**, 383–408, doi:[10.1016/j.dsr2.2004.05.025](https://doi.org/10.1016/j.dsr2.2004.05.025).
- Sheng, J. X., A. Ysasi, E. Kanso, M. Nitsche, and K. Schneider, 2011: Simulating vortex wakes of flapping plates. *Natural Locomotion in Fluids and on Surfaces: Swimming, Flying, and Sliding*, S. Childress et al., Eds., IMA Volumes in Mathematics and its Applications, Vol. 155, Springer, 255–262, doi:[10.1007/978-1-4614-3997-4_21](https://doi.org/10.1007/978-1-4614-3997-4_21).
- Simmons, H. L., and D. Nof, 2002: The squeezing of eddies through gaps. *J. Phys. Oceanogr.*, **32**, 314–335, doi:[10.1175/1520-0485\(2002\)032<0314:TSOETG>2.0.CO;2](https://doi.org/10.1175/1520-0485(2002)032<0314:TSOETG>2.0.CO;2).
- Southwick, O. R., E. R. Johnson, and N. R. McDonald, 2015: A point vortex model for the formation of ocean eddies by flow separation. *Phys. Fluids*, **27**, 016604, doi:[10.1063/1.4906112](https://doi.org/10.1063/1.4906112).
- Tanabe, A., and C. Cenedese, 2008: Laboratory experiments on mesoscale vortices colliding with an island chain. *J. Geophys. Res.*, **113**, C04022, doi:[10.1029/2007JC004322](https://doi.org/10.1029/2007JC004322).
- Walters, R. A., P. A. Gillibrand, R. G. Bell, and E. M. Lane, 2010: A study of tides and currents in Cook Strait, New Zealand. *Ocean Dyn.*, **60**, 1559–1580, doi:[10.1007/s10236-010-0353-8](https://doi.org/10.1007/s10236-010-0353-8).
- Ysasi, A., E. Kanso, and P. K. Newton, 2011: Wake structure of a deformable Joukowski airfoil. *Physica D*, **240**, 1574–1582, doi:[10.1016/j.physd.2011.06.021](https://doi.org/10.1016/j.physd.2011.06.021).